

**Study of  $^{11}\text{B}$  and  $^{13}\text{C}$  NMR on doped  $\text{MgB}_2$  in the normal and in the superconducting state**R. W. Bounds,<sup>1</sup> E. Pavarini,<sup>2,3</sup> M. Paoella,<sup>4</sup> E. Young,<sup>4</sup> I. Heinmaa,<sup>5</sup> R. Stern,<sup>5</sup> and M. Carravetta<sup>1,\*</sup><sup>1</sup>*School of Chemistry, University of Southampton, Southampton SO17 1BJ, United Kingdom*<sup>2</sup>*Institute for Advanced Simulation, Forschungszentrum Jülich, D-52425 Jülich, Germany*<sup>3</sup>*JARA High-Performance Computing, RWTH Aachen, 52062 Aachen, Germany*<sup>4</sup>*Institute of Cryogenics, School of Engineering Sciences, University of Southampton, Southampton SO17 1BJ, United Kingdom*<sup>5</sup>*National Institute of Chemical Physics and Biophysics, Tallinn 12618, Estonia*

(Received 15 June 2017; revised manuscript received 12 September 2017; published 16 January 2018)

We have studied carbon-doped magnesium diboride nanoparticles using  $^{13}\text{C}$  and  $^{11}\text{B}$  NMR in the normal and superconducting states. Measurements of the line shape reveal the role of carbon as a flux-pinning center and, combined with Knight shift measurements, suggest the doping procedure favors the chemical substitution scenario. We perform *ab initio* calculations on a structure with a single carbon-boron substitution which yield results that match the experimental data. The  $^{13}\text{C}$  and  $^{11}\text{B}$  Knight shift data are used to extract the spin susceptibility, which indicates a BCS pairing mechanism; however, we do not observe the Hebel-Slichter coherence peak from  $1/T_1$  data, which we hypothesize is due to a pair-breaking mechanism present in the boron planes.

DOI: [10.1103/PhysRevB.97.014509](https://doi.org/10.1103/PhysRevB.97.014509)**I. INTRODUCTION**

Magnesium diboride,  $\text{MgB}_2$ , is a type-II superconductor with  $T_c = 39$  K discovered in 2001 [1]. This discovery has instigated a wide range of technological and theoretical interest arising from both the novel behavior of double-gapped superconductivity and the search for materials with high critical fields  $H_{c2}$  and high critical-current densities  $J_c$  [2]. The value of  $J_c$  depends on a balance between the Lorentz and pinning forces on vortices; thus there is interest in understanding the mechanism of pinning in order to design better superconductors in the future.

One typical method of enhancing both  $H_{c2}$  and the field dependence of  $J_c$  is by doping  $\text{MgB}_2$  with carbon, which can be achieved by the addition of SiC [3] or  $\text{B}_4\text{C}$  [4]. It is known that carbon acts as a weak flux-pinning center, and  $J_c$  is increased through intrinsic and extrinsic pinning [5,6]. The exact flux-pinning mechanism has not been fully established; however, there are two main scenarios often proposed. The first is that the added C atoms substitute for B sites, leading to distortion of the boron sublattice and a decrease of the  $a$ -axis parameter [7]. Then the increase of  $J_c$  at high fields arises from an enhanced  $H_{c2}$ , brought about by reduced coherence length from distortion of the crystal structure [8]. The second scenario indicates boron vacancies rather than substituted atoms cause the distortion and thereby the enhancement of  $H_{c2}$  and  $J_c$ . In this model the carbon encapsulates unreacted boron and prevents agglomeration. The carbon is therefore outside the

$\text{MgB}_2$  phase, mostly at the grain boundaries, but this has been clearly observed only in a malic-acid-doped sample [9].

One spectroscopic method that can distinguish between these scenarios is NMR, which is well known to be a site-specific local probe. This locality is particularly relevant at temperatures below  $T_c$ , when magnetic flux (from the applied NMR field) begins to penetrate in a periodic fashion. If carbon atoms occupy a different chemical site than boron, then the NMR line shape will differ between  $^{13}\text{C}$  and  $^{11}\text{B}$  NMR. This is especially the case if C atoms truly act as flux-pinning centers; then they will pin the normal conducting vortex core while the material is in the superconducting state.

In the past  $\text{MgB}_2$  has been studied by NMR, with special attention paid to the boron site due to the favorable properties of the highly sensitive and abundant  $^{11}\text{B}$  [10–21], but there have also been studies on the magnesium site via low abundance and the magnetogyric ratio  $^{25}\text{Mg}$  NMR [22] and, if doped with aluminum to replace magnesium, by  $^{27}\text{Al}$  NMR [10,12,23] as well.  $^{13}\text{C}$  NMR has not been utilized up to this point, likely due to the low natural abundance of carbon. However,  $^{13}\text{C}$  isotopic enrichment also makes this doped nucleus quite accessible.

In addition to the role of carbon in flux pinning, there may be additional insights that can be gained from  $^{13}\text{C}$  NMR as now discussed.  $\text{MgB}_2$  is thought to be a nontrivial phonon-mediated BCS superconductor from measurements of a large isotope effect [24] and *ab initio* calculations of the electron-phonon coupling constant [25]. For Al-doped  $\text{MgB}_2$ ,  $^{27}\text{Al}$  NMR results [12] indicate the presence of a Hebel-Slichter coherence peak [26], which is well known to support the  $s$ -wave mechanism. However, there is ambiguity in the  $^{11}\text{B}$  NMR data, possibly due to a peak-suppressing mechanism that may exist in the boron-graphite-like planes. Testing this hypothesis requires, in addition to  $^{11}\text{B}$ , yet another NMR active nucleus which resides in the planes, such as  $^{10}\text{B}$  or, if doped with carbon,  $^{13}\text{C}$  NMR.

In this study we establish the location of carbon in  $\text{MgB}_{2-x}\text{C}_x$  using  $^{11}\text{B}$  and  $^{13}\text{C}$  NMR and also study the

\*m.carravetta@soton.ac.uk

Published by the American Physical Society under the terms of the [Creative Commons Attribution 4.0 International](https://creativecommons.org/licenses/by/4.0/) license. Further distribution of this work must maintain attribution to the author(s) and the published article's title, journal citation, and DOI.

normal and superconducting states to gain further insight into the mechanism of the superconductivity. We determine NMR parameters such as the Knight shift and  $T_1T$  for both  $^{11}\text{B}$  and  $^{13}\text{C}$  and compare our findings to *ab initio* calculations.

## II. MATERIALS AND METHODS

The synthesis of  $\text{MgB}_2$  and  $\text{MgB}_{2-x}\text{C}_x$  was carried out with the liquid-Mg infiltration technique. To produce  $\text{MgB}_2$ , a magnesium rod (Sigma-Aldrich) and boron powder (Speciality Materials Inc.) were mixed in a superstoichiometric B-Mg ratio of 1:1.35 and placed in tantalum foil, which was crimped shut and heated to 850 °C for 10 h.

Carbon doping was achieved by chemical vapor deposition (CVD), a method which allows uniform distribution of carbon onto a boron precursor, using a purpose-built stainless-steel tube furnace for CVD of carbon on boron powder [7], which then reacted with a nanoboron powder. The carbon-doped  $\text{MgB}_{2-x}\text{C}_x$  was prepared by reacting 99% enriched  $^{13}\text{C}_2$ -ethylene gas (Sigma-Aldrich) with boron powder to form the  $^{13}\text{C}$ -doped boron precursor. The furnace tube was evacuated using a turbomolecular pump to  $10^{-4}$  mbar; then ethylene gas was introduced, and the boron powder was treated for fixed periods. These carbon-doped boron precursors were also subjected to liquid-Mg infiltration treatment with Mg rods at 850 °C for 10 h, using the same procedure as for the undoped materials. The samples were characterized by a number of methods in order to establish sample purity and homogeneity, particle size, and magnetic properties.

## III. CHARACTERIZATION OF THE SAMPLE

$\text{MgB}_2$  consists of a hexagonal  $\text{AlB}_2$  graphite-type structure with space group  $P6/mmm$ . To establish purity and investigate the location of carbon upon doping, powder x-ray diffraction (XRD) measurements were performed on a Bruker D2 Phaser using  $\text{Cu } K\alpha_{1/2}$  radiation with  $\lambda = 1.5418 \text{ \AA}$ . The change in the  $\mathbf{a}$ -axis lattice parameter was calculated from the angular shift of the (100) reflection, which, when inserted in Bragg's equation, gives the spacing between the planes in the atomic lattice  $d$ . The  $\mathbf{a}$ -axis lattice parameter was then calculated, considering that  $\text{MgB}_2$  adopts a hexagonal structure, with the following relation:  $a = d / \cos(30^\circ)$ . The carbon content  $x$  of samples,  $\text{MgB}_{2-x}\text{C}_x$ , was estimated by using an empirical result for the single crystals, which is consistent with data points plotted as the shift in the  $\mathbf{a}$  axis against  $x$ .

Calculations from the shift of the (100) reflection in powder XRD measurements (data not shown) are compatible with a carbon doping of approximately 5% [7]. Previous works have shown the linear relationship between the doping level and change in the  $\mathbf{a}$ -axis parameter [27], also interpreted as evidence that boron is replaced by carbon in the lattice. However, it has also been noted that the change in  $a$  may be due to boron vacancies rather than carbon substitutions [9]; therefore we must use NMR to fully establish the dopant location.

The level of carbon enrichment is further confirmed by measurements of the magnetic susceptibility of the sample as a function of temperature, as shown in Fig. 1(a) using the vibrating sample magnetometer option of the Quantum Design

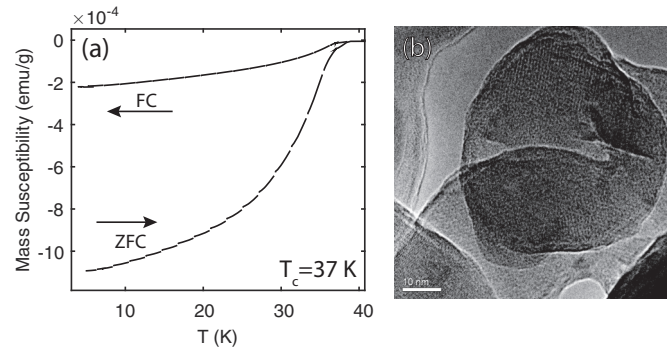


FIG. 1. (a) Magnetic-susceptibility measurements on  $\text{MgB}_{1.95}\text{C}_{0.05}$ .  $T_c$  was determined to be 37 K at 0.01 T. (b) TEM images of carbon chemical-vapor-coated  $\text{MgB}_{1.95}\text{C}_{0.05}$  powder particles reacted at 850 °C.

physical property measurement system equipped with a 14-T solenoid. The zero-field critical temperature  $T_c$  was measured [Fig. 1(a)] from the onset of the diamagnetism in zero-field cooling (ZFC). The ZFC susceptibility measurements indicate  $T_c = 37 \text{ K}$  in a field of 0.01 T, and this is in good agreement with previous studies of carbon-doped  $\text{MgB}_2$  with doping at  $\approx 5\%$  [7]. The doped sample was also characterized using transmission electron microscopy (TEM) measurements, as shown in Fig. 1(b). An estimate of average particle size is 100 nm using this method.

## IV. NMR SPECTROSCOPY

The room-temperature magic-angle-spinning (MAS) NMR data were acquired on a 9.4-T Bruker Ascend 400WB spectrometer and a Chemagnetics CMX Infinity console, with nitrogen flow for bearing and drive gases, and on a 14.1-T Bruker Avance-II 600WB spectrometer. At 9.4 T a 40-mg sample was packed into a 4-mm zirconium oxide rotor and spun at 8 kHz to obtain MAS and multiple quantum MAS (MQMAS) spectra of  $^{11}\text{B}$  in the doped  $\text{MgB}_{2-x}\text{C}_x$  and undoped materials. The 3QMAS spectra were obtained using the  $z$ -filtered method discussed in Ref. [28]. The  $^{13}\text{C}$  spectra were recorded under MAS at 14.1 T, with 10 mg of  $\text{MgB}_{2-x}\text{C}_x$  packed into a 2.5-mm rotor and spun at 30 kHz. MAS spectra were recorded using a Hahn echo [29] pulse sequence with an 80-kHz amplitude pulse and an echo delay with  $\tau = 50 \mu\text{s}$ .

Double-quantum  $^{13}\text{C}$ - $^{13}\text{C}$  recoupling experiments using the symmetry  $\text{R}20_2^9$  were performed at 14.1 T at a spin rate of 10 kHz with a spin echo at the end of the double-quantum (DQ) reconversion period. The sequence used mixing times in the range of 10 to 250  $\mu\text{s}$ , which are suitable to detect  $^{13}\text{C}$ - $^{13}\text{C}$  correlations between atoms in close proximity.

Cryogenic  $^{11}\text{B}$  and  $^{13}\text{C}$  NMR experiments were performed on 4.7 and 8.5 T wide-bore magnets using an upgraded Bruker AMX 360 console. All experiments were run static using a helium gas flow cryostat from Janis Research Inc. The temperature was measured using a calibrated Lakeshore Cernox sensor, with an accuracy of at least 0.1 K, placed within proximity of the sample.  $\text{MgB}_2$  powders were stored and handled in an argon glove box with oxygen and moisture levels less than 0.5 ppm. Cryogenic  $^{11}\text{B}$  NMR measurements were

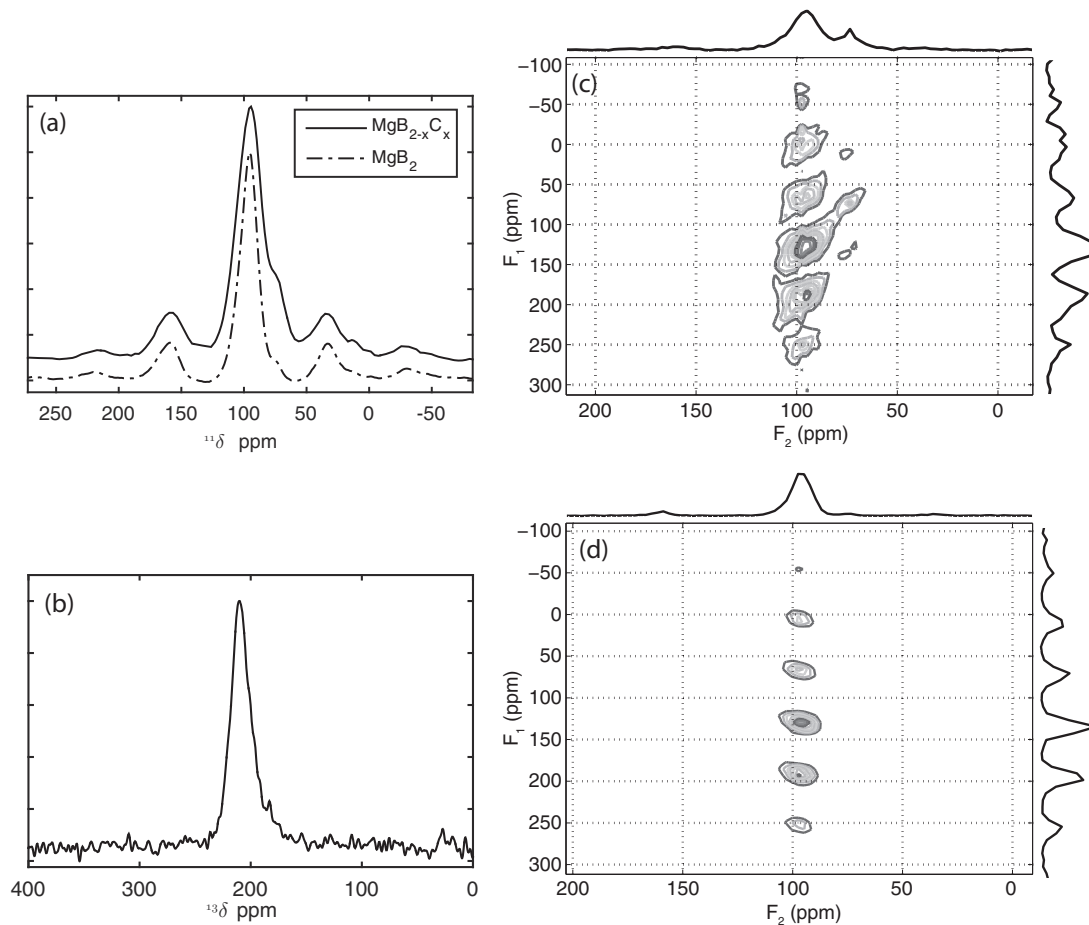


FIG. 2. (a)  $^{11}\text{B}$  MAS-NMR direct acquisition spectrum recorded with 80-kHz pulse amplitude; spectra are the result of 40 transients with 4 s between scans, and the sample is in a 4.0-mm rotor, spinning at 8 kHz in a constant field of 9.4 T. (b)  $^{13}\text{C}$  MAS-NMR spectrum recorded with 80-kHz pulse amplitude and a Hahn echo sequence with  $\tau = 50 \mu\text{s}$ ; the spectrum is the result of 131 000 transients with 1 s between scans on 10 mg of  $\text{MgB}_{1.95}\text{C}_{0.05}$  packed into a 2.5-mm zirconium oxide rotor spinning at 30 kHz at 14.1 T. (c) MQMAS spectrum of  $\text{MgB}_{1.95}\text{C}_{0.05}$ . (d) MQMAS spectrum of  $\text{MgB}_2$ .

performed on 43 mg of  $\text{MgB}_{1.95}\text{C}_{0.05}$  packed into a 4-mm zirconium oxide rotor. Relaxation data were obtained using saturation recovery experiments with a comb of 80 pulses, with  $\pi/2$  pulse durations of 1.25  $\mu\text{s}$  and 16 or 32 elements in the variable delay list.

All  $^{11}\text{B}$  NMR data were referenced to Boron trifluoride diethyl etherate ( $\text{BF}_3\text{OEt}_2$  (aq)) at 0 ppm. The quadrupolar coupling constant  $C_q$  is assumed to be 835 kHz, as reported in previous studies [23]. Carbon was referenced to adamantane with a chemical shift of 38.23 ppm ( $\text{CH}_2$  peak) [30].

## V. ROOM-TEMPERATURE MAS-NMR EXPERIMENTS

The  $\text{MgB}_{1.95}\text{C}_{0.05}$  sample was characterized by MAS-NMR using the advantage of MAS of producing spectra with higher resolution when compared to static NMR. The improved resolution comes from partial suppression of anisotropic NMR interactions such as the Knight shift, chemical shift, dipole-dipole couplings, and first-order quadrupolar effects. Second-order quadrupolar effects still remain and are inversely related to the applied magnetic field strength.

MAS-NMR allows characterization of the chemical nature of each isotopic species and reveals the presence of impurities

and inequivalent sites through the presence of additional peaks. The boron MAS-NMR spectrum for the central transition ( $-1/2 \rightarrow +1/2$ ) of the spin-3/2  $^{11}\text{B}$  nucleus in  $\text{MgB}_2$  and  $\text{MgB}_{1.95}\text{C}_{0.05}$  is shown in Fig. 2(a). The main peak is centered at 95 ppm, and the peak position has a contribution from the second-order isotropic quadrupolar shift. Prolonged exposure of  $\text{MgB}_2$  in air would result in  $\text{B}_2\text{O}_3$  impurities that would manifest as an additional resonance at 0 ppm. No such signal is seen in Fig. 2(a), indicating the samples are high purity and have not been exposed in air.

The asymmetry of the  $^{11}\text{B}$  line shape is due to the second-order quadrupole interaction, the anisotropic Knight shift, and the dipolar interaction. On the doped sample the asymmetry is more prominent with the presence of a second boron environment due to the slightly different environment experienced by boron nuclei in proximity to the  $^{13}\text{C}$  dopants. This may indicate the carbon-boron substitution model is correct and that the boron vacancy model is not because in the latter model, the  $^{11}\text{B}$  NMR signal would be expected to be similar to the undoped  $\text{MgB}_2$ . This is because the boron network should remain relatively undisturbed, and therefore no additional boron carbide sites would be observed through  $^{11}\text{B}$  NMR. A mix of models would give additional peaks in the

$^{13}\text{C}$  MAS-NMR spectrum; however, only one carbon site is observed, as shown in Fig. 2(b). The magnetic shift is  $200 \pm 5$  ppm and is reflective of the local electronic environment. Even at a 30-kHz MAS spinning rate, the linewidth is 2.8 kHz, which may largely arise from heterogeneity of the  $^{13}\text{C}$  environments and some level of residual heteronuclear dipolar interaction with the boron nuclei. There are no other obvious carbon sites, and as there is an additional boron shoulder, this may indicate boron-carbon substitution is the most likely model after the CVD procedure of synthesis.

As  $^{11}\text{B}$  is a spin-3/2 nucleus, the NMR spectrum is complicated by the presence of the quadrupolar interaction, which causes additional line broadening. Higher resolution may be gained by using the MQMAS experiment [28]. Figure 2(d) shows the MQMAS spectrum of  $\text{MgB}_2$ . It is clear that there is only one  $^{11}\text{B}$  site, as expected. Figure 2(c) shows MQMAS data collected for the  $\text{MgB}_{2-x}\text{C}_x$  sample; the peak associated with the boron sublattice is broadened but has the same position as in  $\text{MgB}_2$ , indicating some level of disorder but very similar shift and quadrupolar parameters. Additionally, there is a well-resolved second peak which appears near 70 ppm which is likely to be a boron carbide site, as noted previously.

In order to investigate carbon clustering, double-quantum  $^{13}\text{C}$ - $^{13}\text{C}$  recoupling experiments were performed (data not shown). After approximately 60 000 scans there was no evidence of a signal, putting an upper threshold on the DQ excitation efficiency for that condition at 0.6% (obtained by taking the ratio between the integrated signal intensity in the DQ and conventional spin-echo experiments after normalizing to the same number of scans), indicating that the  $^{13}\text{C}$  signal comes almost entirely from isolated  $^{13}\text{C}$  sites.

## VI. CRYOGENIC NMR EXPERIMENTS ON $\text{MgB}_{1.95}\text{C}_{0.05}$

In a type-II superconductor, different nuclei are subject to the various local fields based on the position with respect to the flux lines in the superconducting state [31]. The role played by carbon atoms in the superconducting state can therefore be derived by following the  $^{13}\text{C}$  and  $^{11}\text{B}$  NMR spectra as a function of temperature, as shown in Fig. 3. For each temperature, spectra obtained at 8.5 and 4.7 T are superimposed for each isotopic species. Spectra are reported only from 80 K and below as there were no significant variations in peak shape and position above this temperature.

At temperatures higher than  $T_c$  the material is in the normal state, and both  $^{11}\text{B}$  and  $^{13}\text{C}$  spectra consist of a relatively narrow, slightly asymmetric line. At 8.5 T the  $^{13}\text{C}$  and  $^{11}\text{B}$  NMR line shapes develop a more prominent asymmetry in the superconducting state; simultaneously, the magnetic shift changes, reflective of the pairing of electrons and the drop in spin susceptibility. This behavior is also observed at 4.7 T; however, there is also a significant broadening due to a mixture of the inhomogeneous distribution of magnetic fields arising from the vortex state and diamagnetic screening currents [32].

The extent of this effect varies between nuclei; for example,  $^{11}\text{B}$  at 4.7 T shown in Fig. 3(a) shows a large shift in peak position and an increase in linewidth, as the shift is field independent, whereas data at 8.5 T show only a modest change in peak position, which can be attributed to the inhomogeneous field distribution arising from the vortices in the solid phase

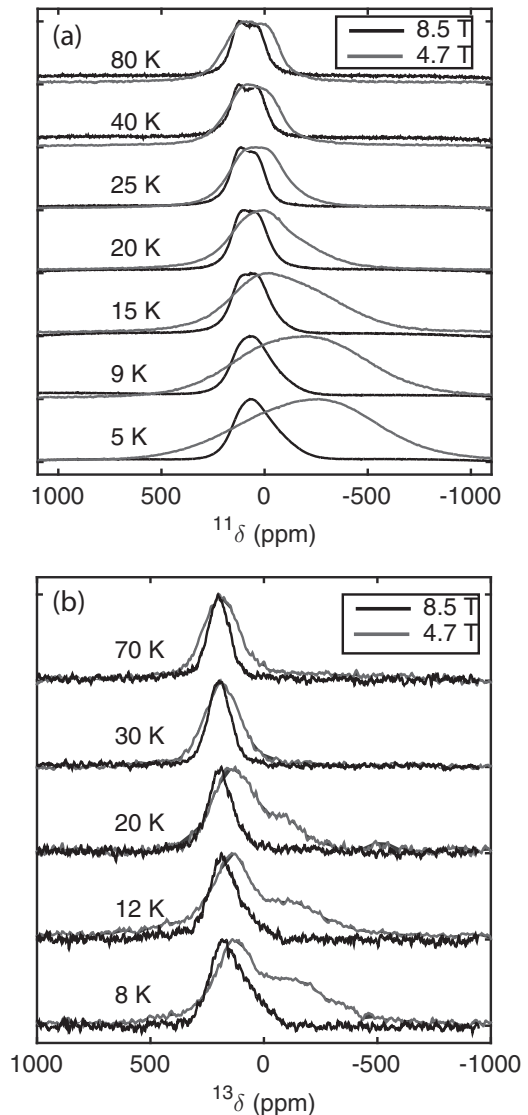


FIG. 3. NMR peak shape of  $\text{MgB}_{1.95}\text{C}_{0.05}$  as a function of temperature. (a)  $^{11}\text{B}$  NMR spectra at fields of 8.5 and 4.7 T. (b)  $^{13}\text{C}$  NMR spectra at fields of 8.5 and 4.7 T.

[31,33–35]. This is expected as the magnetic field distribution is less densely packed and there are larger field gradients in lower external magnetic fields [13].

The case is not the same for  $^{13}\text{C}$  data in Fig. 3(b), which show the normal-state signal persisting below  $T_c$  and a relatively smaller vortex field distribution. As nuclei are subject to local fields based on the position with respect to the flux lines [31], this line shape is likely due to carbon's role as a flux-pinning site, closer to the normal-state vortex core, and this manifests at  $T < T_c$  in the spectra as a more persistent normal-state signal. The line shapes are, in general, broad, which is due to the anisotropic NMR interactions in polycrystalline samples, and this means extracting quantitative information is difficult. There are better techniques, such as muon spin relaxation [36,37], which allow one to obtain quantitative information from the line shape such as the penetration depth, and they are usually modeled using Brandt's method [38].

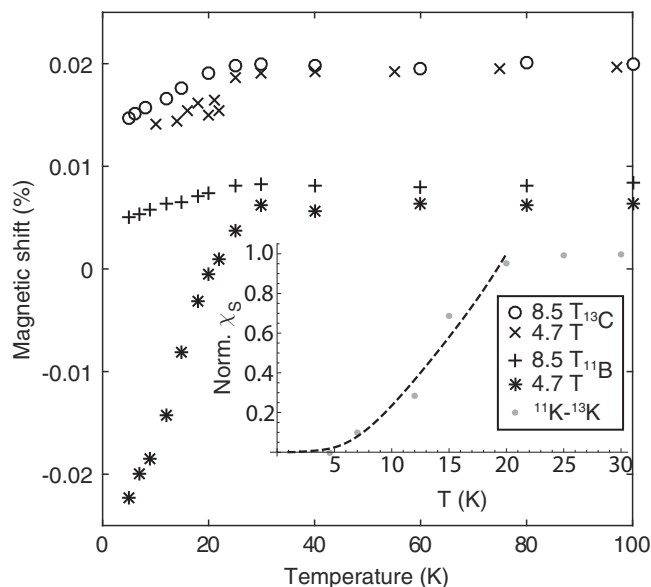


FIG. 4. Knight shift (%) of  $^{13}\text{C}$  and  $^{11}\text{B}$  on  $\text{MgB}_{1.95}\text{C}_{0.05}$  as a function of temperature at 4.7 and 8.5 T. Normalized spin susceptibility was obtained by subtracting Knight shifts as described in text.

The conduction electrons in a metal exert a magnetic field on the nuclei, and this is observed in the NMR spectrum as a shift in frequency, known as the Knight shift. As the shift arises from the nuclear hyperfine coupling, it is intimately linked with the superconducting mechanism. In order to probe the electronic structure of  $\text{MgB}_{1.95}\text{C}_{0.05}$  further, we studied the Knight shift at various temperatures in the normal and superconducting states. Figure 4 shows the dependence of the magnetic shift as a function of temperature for both boron and carbon. The difference in magnitude of  $^{11}\text{B}$  between fields can be ascribed to the diamagnetic Meissner screening currents, which are field dependent. The inhomogeneous field distribution in the vortex state is well resolved in  $^{13}\text{C}$  NMR; therefore we are able to follow the temperature dependence of the normal-state signal, which broadly follows a similar temperature dependence at both 4.7 and 8.5 T.

The decrease in shift at low temperatures can be assigned to the Knight shift decay, which is independent of the magnetic field. The Knight shift can be approximated for both  $^{13}\text{C}$  and  $^{11}\text{B}$  by taking the difference between the normal-state shift and the lowest-temperature shift. The assumption of this method is that the lowest temperature is within the zero slope of the Knight shift decay; therefore only  $\alpha K_{\text{orbital}}$  (and if  $I > 1/2$ , then also  $\alpha K_Q$ ) remains. However, this is an approximation because it is unknown if the data lie within the true zero slope of the Knight shift decay. This procedure is done using data at 8.5 T, yielding  $^{13}K_{\text{spin}} = 0.0061 \pm 0.0008\%$  ( $61 \pm 8$  ppm) and  $^{11}K_{\text{spin}} = 0.0036 \pm 0.0005\%$  ( $36 \pm 5$  ppm). The Knight shift for boron is broadly in line with previous studies which report  $K_{\text{spin}} = 40$  ppm when  $^{11}\text{B}$  is referenced to  $\text{BF}_3\text{OEt}_3$  [23]. We used data at 8.5 T because the Knight shift is independent of field but the diamagnetic contribution has an inverse dependence; this property is more prominent in  $^{11}\text{B}$  data than in  $^{13}\text{C}$ , although there is still a small shift at low temperature between fields. This is strong evidence that boron spins are within the magnetic field gradients in the vortex field

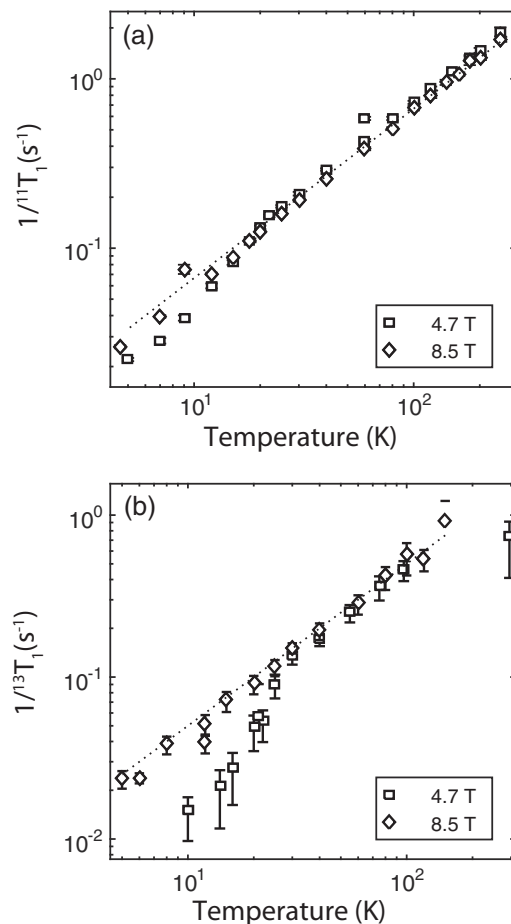


FIG. 5. Spin-lattice relaxation rate of  $\text{MgB}_{1.95}\text{C}_{0.05}$ . (a)  $^{11}\text{B}$  NMR. (b)  $^{13}\text{C}$  NMR. The black dotted line is the Korringa product. Values are 155 and 200 s K for boron and carbon, respectively.

distribution, whereas carbon spins occupy mainly the vortex cores because they act as flux-pinning centers.

A comparison of local electronic structure between  $^{13}\text{C}$  and  $^{11}\text{B}$  can also be made by measuring the nuclear spin-lattice relaxation rate ( $1/T_1$ ) as a function of temperature, as shown in Fig. 5. Both  $^{11}\text{B}$  and  $^{13}\text{C}$  nuclei show a linear temperature dependence in the normal phase, which is typical for metallic systems and is more commonly known as Korringa's law [39]; at  $T = T_c$  there is a deviation from the linear dependence, and the relaxation time becomes longer. Figure 5(a) shows  $1/T_1$  for  $^{11}\text{B}$  nuclei; we find  $T_1 T = 155 \pm 10$  s K, which is consistent with studies on powders [11, 18, 23, 40, 41] and single crystals [15]. Figure 5(b) shows  $1/T_1$  for  $^{13}\text{C}$  nuclei,  $T_1 T = 200 \pm 20$  s K. As the temperature is lowered below  $T_c$ ,  $1/T_1$  deviates from Korringa's law; the coherence peak [26] is not observed, which may be due to a pair-breaking mechanism due to the static magnetic field present, as hypothesized previously [11]. In boron this deviation is enhanced by the presence of a dopant (carbon), as seen in previous works [14, 18].

$T_1$  and the Knight shift both depend on the electron-nuclear hyperfine interaction, and they are related by the Korringa ratio, which is dimensionless and given by

$$K_s^2 T_1 T = \frac{\hbar}{4\pi k_B} \frac{\gamma_e^2}{\gamma_n^2} \equiv S, \quad (1)$$

where  $k_B$  is the Boltzmann constant,  $\gamma_n$  and  $\gamma_e$  are the gyromagnetic ratios for nuclei and electrons, respectively,  $K_s$  is the Knight shift, and  $T_1$  is the nuclear spin-lattice relaxation time. This equation is usually used as a ratio,  $R = T_1 T K_s^2 / S$ . A Fermi liquid will typically have  $R$  close to unity; however, real materials often deviate from this value.  $T_1 T$  can be enhanced by ferromagnetic or antiferromagnetic correlations, whereas only ferromagnetic correlations can enhance the Knight shift. This means that the deviation of  $R$  from unity yields information about which type of correlation is important, with  $R > 1.0$  implying antiferromagnetic electronic correlations and  $R < 1.0$  implying ferromagnetic correlations.

Taking the Knight shift to be  $^{11}\text{K}_s = 31\text{--}41$  ppm for  $^{11}\text{B}$ , we find  $R = 0.08 \pm 0.02$ , which agrees with previous reports [23] but is lower than the value  $R = 0.2$  reported in Refs. [11,15]. The Korringa ratio for  $^{13}\text{C}$ , using  $^{13}\text{K}_s = 53\text{--}69$  ppm, is  $R = 0.18 \pm 0.07$ .  $^{27}\text{Al}$  measurements reported previously for  $\text{Mg}_{1-x}\text{Al}_x\text{B}_2$  indicate that while  $R \approx 1$  for pure  $\text{AlB}_2$ , i.e., the ideal value of unity for  $s$  electrons,  $R \approx 0.5$ , for superconducting samples ( $x \leq 0.6$ ), indicating a considerable orbital contribution to the relaxation rate [10].

## VII. SPIN SUSCEPTIBILITY

A useful approach to test the appropriateness of the BCS picture is to measure the spin susceptibility, which allows extraction of the BCS gap at zero temperature  $\Delta_0$  by fitting it to the Yosida function [42]. To do this one must carefully decompose the magnetic shift into a series of contributions as summarized below:

$${}^\alpha K_{\text{total}} = {}^\alpha K_{\text{spin}}(T) + {}^\alpha K_{\text{orbital}} + {}^\alpha K_Q + \Delta B / B_0, \quad (2)$$

where  ${}^\alpha K_{\text{spin}}$  and  ${}^\alpha K_{\text{orbital}}$  represent the Knight and chemical shifts, respectively,  $\alpha$  is the nuclear isotope, and  $K_Q$  is the isotropic shift from the second-order quadrupolar interaction.  $\Delta B / B_0$  represents the diamagnetic shift which arises from Meissner screening currents in the superconducting state. The relevant term in the analysis of the superconducting state is the Knight shift, which can be analyzed as

$${}^\alpha K_{\text{spin}} = \vec{A} \chi^S, \quad (3)$$

where  $\vec{A}$  is the hyperfine coupling tensor and  $\chi^S$  is the dimensionless Pauli spin susceptibility [43]. The temperature dependence of  $\chi^S(T)$  cannot be measured directly because of the Meissner screening currents in the vortex state, which are, in general, much greater than the Knight shift and are field dependent. There are also orbital and quadrupolar contributions to the shift, but these act as a temperature-independent offset for each nuclear species and can be ignored in following procedure. The diamagnetic shift from the screening currents may be removed by subtracting total shifts of two isotopic nuclear species using Eq. (3) as follows:

$${}^{11}\text{K}_{\text{total}}(T) - {}^{13}\text{K}_{\text{total}}(T) = (A_{11} - A_{13})\chi^S(T). \quad (4)$$

The resulting quantity is the spin susceptibility, scaled by the difference between hyperfine coupling tensors, and therefore requires normalization. This quantity can then be fitted with a Yosida function, which depends upon the superconducting energy gap. To calculate the Yosida function for two gaps, we

use

$$Y(T) = \beta Y_1(T) + (1 - \beta)Y_2(T), \quad (5)$$

with the Yosida function based on Ref. [44] as follows:

$$\frac{K_s(T)}{K_s(T_c)} = Y_i(T) = 1 - 2\pi k_B T \sum_{n=0}^{\infty} \frac{\Delta^2(T)}{[\epsilon_n^2 + \Delta^2(T)]^{2/3}}, \quad (6)$$

where  $K_s(T)$  is the Knight shift,  $k_B$  is the Boltzmann constant,  $\Delta$  is the superconducting gap, and  $\epsilon_n = 2\pi(n + 1/2)k_B T$ . We calculate the superconducting gap using

$$\Delta(T) = \Delta(0) \tanh \left[ \frac{k_B T c \pi}{\Delta(0)} \sqrt{\frac{2}{3} \left( \frac{T_c}{T} - 1 \right) \frac{\Delta C}{C}} \right], \quad (7)$$

where  $\frac{\Delta C}{C} = 1.43$ . We extracted the spin susceptibility from the Knight shifts as discussed above and fit the experimental data to a Yosida function with two superconducting gaps, as shown in the inset of Fig. 4. This method yields superconducting gap ratios of  $2\Delta/k_B T_c = 3.15 \pm 0.1$  ( $\beta = 0.94$ ) and  $2\Delta/k_B T_c = 1.0 \pm 0.5$  ( $\beta = 0.06$ ). We note that the fit was determined almost completely by the first gap value, which is close to the usual BCS gap ratio of 3.53. In pure  $\text{MgB}_2$ , tunneling spectroscopy [45,46] studies report two gaps related to  $\sigma$  and  $\pi$  bands with superconducting gap ratios of  $2\Delta/k_B T_c = 5\text{--}6$  and  $1.2\text{--}1.5$ , respectively. Similarly, point-contact spectroscopy [47] gives  $2\Delta/k_B T_c = 4.1$  and  $1.7$ .

The two-band nature of  $\text{MgB}_2$  is thought to be preserved upon doping with carbon in polycrystalline materials up to  $x = 0.10$ . However, we find the isotropic gap function more appropriately fits the data in this case, and it has been noted previously that increased interband scattering can lead to effectively one-band behavior due to merging of the superconducting gaps to an average value [12]. This observation is consistent with the gap ratio value measured here. Other tunneling measurements have suggested that the carbon dopant actually suppresses interband scattering, which means the two gaps are preserved [48]. It is not obvious why NMR seems to yield different, single-gap behavior, but this difference has also been noted before when determining the gap using  $^{11}\text{B}$   $1/T_1$  measurements in pure  $\text{MgB}_2$  [49].

## VIII. FIRST-PRINCIPLES CALCULATIONS OF KNIGHT SHIFTS AND THE RELAXATION RATE

We calculate the Knight shift and the relaxation rate *ab initio* by using the approach described in Refs. [23,50,51]. It is based on the density-functional theory in the local-density approximation and the linearized muffin-tin orbital method (STUTTGART LMTO47 code). In the past this approach has been

TABLE I. Experimental static  $^{13}\text{C}$  and  $^{11}\text{B}$  NMR parameters for  $\text{MgB}_{1.95}\text{C}_{0.05}$ . The Korringa ratio  $R$  is defined as  $R = T_1 T K_s^2 / S$ .

	$^{11}\text{B}$	$^{13}\text{C}$
$K$ (ppm)	$36 \pm 2$	$61 \pm 8$
$1/T_1 T$ ( $10^{-3}/\text{K s}$ )	$6.5 \pm 4$	$5.0 \pm 5$
$S$ (s K)	$2.57 \times 10^{-6}$	$4.17 \times 10^{-6}$
$R$	$0.08 \pm 0.02$	$0.177 \pm 0.69$

TABLE II. Calculated dipole-dipole, contact, and core contributions to the Knight shift in  $\text{MgB}_{2-p}\text{C}_p$  (in ppm). The label  $\alpha = xy, z$  indicates the direction of the applied external magnetic field. In the last column the average shift (i.e., the total for powder samples) is given.

$p$	Element	Dipole- $xy$	Dipole- $z$	Contact	Core	Average
0.125	C	-24	48	34	33	67
0.125	B	$-8.0 \pm 4.0$	$16 \pm 8.0$	$30 \pm 12.5$	$-14 \pm 7$	21
0.083	C	-23	46	35	29	54
0.083	B	$-11 \pm 5.0$	$22 \pm 1.0$	$35 \pm 13$	$-9 \pm 3$	24

successfully used to calculate Knight shift and relaxation rates for  $\text{MgB}_2$ ,  $\text{AlB}_2$ , and other materials. Here, in order to study the effects of  $^{13}\text{C}$  substitution, we perform calculations for several supercells, with carbon replacing boron on the boron sublattice. In the absence of detailed experimental information on the position of C atoms in the material, we chose large supercells with a single C atom in order to minimize the C-C interactions. In all cases examined, we find a distribution of values for boron sites, in line with the experimental results presented in Table I. In Tables II (Knight shift) and III (relaxation rate) we give the theoretical results for  $^{13}\text{C}$  and  $^{11}\text{B}$ , after averaging over the B sites for the latter; we also give the deviation from the mean as an error bar to give an impression of the distribution of values. Let us now discuss the results starting from the Knight shift (Table II). We find that, among the contributions from the Fermi surface, the Fermi contact is the dominant term for  $^{11}\text{B}$ . For  $^{13}\text{C}$  the Fermi-contact contribution to the Knight shift is similar in magnitude, but the dipole-dipole term dominates (the difference between the contact and dipole-dipole terms is, however, small). A similar result has been reported before for  $^{13}\text{C}$  in the case of fullerenes [52]. The reason is the following. The contact term measures the partial density of states of  $s$  electrons at the Fermi level  $N_s$ , i.e.,  $K^{\text{con}} = \mu_B^2 \frac{4}{3} N_s |\phi_s(0)|^2$ , where  $\phi_s(0)$  is the radial  $s$  wave function at the nuclear site. This term typically dominates because of the large  $|\phi_s(0)|^2$  prefactor; however, in the case of  $\text{MgB}_{1.95}\text{C}_{0.05}$ , for both boron and carbon, the  $s$  partial density of states  $N_s$  is small compared to the  $p$  contribution. Thus the contact term becomes comparable to the dipole-dipole term. The latter is proportional to the difference in the density of states of  $p$  electrons,

$$K_z^{\text{dip}} \sim \frac{4\mu_B^2}{5} (2N_z - N_x - N_y) \langle r^{-3} \rangle_{l=1},$$

where  $\langle r^{-3} \rangle_{l=1} = \langle \phi_p | r^{-3} | \phi_p \rangle$  and  $\phi_p(r)$  is the radial  $p$  wave function. We find that both the difference  $(2N_z - N_x - N_y)$ , a measure of the system anisotropy, and the weight  $\langle r^{-3} \rangle_{l=1}$ , a

measure of  $p$ -electron localization, are, on average, larger for C than for B. We also find that the  $^{13}\text{C}$  Knight shift changes little on increasing the amount of carbon, while the change is slightly larger for  $^{11}\text{B}$ . The final  $^{11}\text{B}$  Knight shifts are not far from the values for pure  $\text{MgB}_2$  [50].

Let us now discuss the effect of core polarization. In order to calculate the latter we apply an external magnetic field  $H$  and calculate the corresponding contribution to the Knight shift as

$$K_{\text{cp}} = \mu_B \frac{8\pi}{3} \sum_n \frac{m_n(0)}{H},$$

where  $n$  is the  $n$ th core shell at the nucleus. For  $^{11}\text{B}$  and  $^{13}\text{C}$  the contribution of the  $1s$  and  $2s$  shells tend to cancel each other, so that the core contribution is small. It is, however, comparable with the contact term; this happens because the latter is relatively small in the compounds analyzed, as previously discussed. Table II shows that including  $K_{\text{cp}}$  improves the comparison with experiments.

Table III presents the theoretical values of  $1/T_1 T$ , where the two dominant contributions for  $^{11}\text{B}$  are the orbital term and the dipole-dipole term, both stemming from B  $p$  states. The same is true for  $^{13}\text{C}$ . In line with the Knight shift results, the value of the relaxation rate for  $^{13}\text{C}$  increases with the amount of carbon per formula unit; in particular the orbital part becomes dominant when  $p$  increases. The theoretical relaxation rates are in rather good agreement with the experimental values in Table I, particularly taking into account that it is impossible to perfectly match experimental and theoretical carbon contents and that the actual positions of carbon atoms and possible associated local distortions are unknown. Experimentally, we find a sizable relaxation rate anisotropy for both  $^{13}\text{C}$  and  $^{11}\text{B}$ ; we determined the latter by integrating in 80-ppm strips across the NMR line shape. The anisotropy is larger for  $^{13}\text{C}$  than for  $^{11}\text{B}$ . This is also in line with our theoretical results, which show that for  $^{13}\text{C}$  the dipole-dipole contribution is about one half of the orbital one, while in the case of boron it is about one third. Finally, we performed another set of calculations with two carbons per supercell, with the carbon neighbors either in the same ring or in different planes. While the contact terms do not change very much, we find that the orbital and dipole contributions tend to sizably increase; for example, for  $p \sim 0.11$  the boron orbital term is  $5.65 \cdot 10^{-3}/(\text{K s})$ , while the dipole one is about  $2.96 \cdot 10^{-3}/(\text{K s})$ . This will lead to a large overestimation of the total relaxation rate. Although we cannot exclude that other types of clustering and supercells might lead to results more in line with experiments, our results indicate that calculations in which carbon atoms are farther apart provide better agreement with experiments.

TABLE III. Calculated relaxation rate  $1/T_1 T$  for  $\text{MgB}_{2-p}\text{C}_p$  [in units of  $(\gamma_n/\gamma)^2 10^{-3}/(\text{K s})$ ]. The last column gives the value to compare with experiments, i.e., the total relaxation rate [in units of  $10^{-3}/(\text{K s})$ ].

$p$	Element	Orbital	Dipole	Contact	Core	Total
0.125	C	4.40	1.86	0.57	0.53	3.65
0.125	B	$3.30 \pm 1.15$	$1.08 \pm 0.2$	$0.62 \pm 0.27$	$0.10 \pm 0.03$	4.00
0.083	C	1.80	1.10	0.60	0.42	1.92
0.083	B	$3.25 \pm 1.35$	$1.13 \pm 0.16$	$0.62 \pm 0.23$	$0.05 \pm 0.00$	4.02

## IX. CONCLUSION

We studied  $^{13}\text{C}$ -doped  $\text{MgB}_2$  powders using a combination of NMR methods and first-principles calculations in order to establish the nature of the  $^{13}\text{C}$  doping sites and obtain further information on the superconducting mechanism using  $^{13}\text{C}$  NMR.

There is a good match between static  $^{13}\text{C}$  and  $^{11}\text{B}$  NMR data for  $\text{MgB}_{1.95}\text{C}_{0.05}$  and *ab initio* calculations, which assume a single carbon substituted for boron in  $\text{MgB}_{2-x}\text{C}_x$ . This result suggests that carbon doping via the CVD method produces a sample with chemically substituted boron rather than defects and the agglomeration of carbon around unreacted boron at the grain boundary. The chemical substitution model being further supported by an additional resolved peak in  $^{11}\text{B}$  via MAS-NMR spectra at room temperature which we assign to a boron carbide site. The double-quantum recoupling experiments suggest carbon does not cluster upon boron substitution. The variable-temperature  $^{13}\text{C}$  NMR experiments below  $T_c$  indicate carbon acts as a flux-pinning center, although we are not able to comment on the balance between other flux-pinning mechanisms such as stacking faults created by boron deficiencies.

The coherence peak is not observed in either  $^{11}\text{B}$  or  $^{13}\text{C}$  NMR, indicating the pair-breaking mechanism hypothesized

previously may be specific to the boron planes [11]. The spin susceptibility extracted from the Knight shifts of  $^{13}\text{C}$  and  $^{11}\text{B}$  NMR allow us to determine the superconducting gap ratios by fitting the decay to the Yosida function. We find the superconducting gap ratios are  $2\Delta/k_B T_c = 3.15 \pm 0.1$  and  $2\Delta/k_B T_c = 1.0 \pm 0.5$ , with the fit almost completely determined by the magnitude of the first gap. It is likely that the two-band nature of  $\text{MgB}_2$  is preserved upon doping, but it has been hypothesized that increased interband scattering leads to effectively one-band behavior due to merging of the gaps to an average value.

## ACKNOWLEDGMENTS

Calculations were done on the Jülich supercomputer Ju-reca. E.P. acknowledges financial support via the Deutsche Forschungsgemeinschaft, research training group RTG1995. Experiments in Tallinn were supported by Institutional Research Grants No. IUT23-7 and No. IUT23-3 of the Estonian Ministry of Education and Research and by the European Regional Development Fund project TK134. M.C. thanks the Royal Society for a University Research Fellowship.

- 
- [1] J. Nagamatsu, N. Nakagawa, T. Muranaka, Y. Zenitani, and J. Akimitsu, *Nature (London)* **410**, 63 (2001).
- [2] D. Kasinathan, K.-W. Lee, and W. Pickett, *Phys. C (Amsterdam, Neth.)* **424**, 116 (2005).
- [3] S. X. Dou, A. V. Pan, S. Zhou, M. Ionescu, H. K. Liu, and P. R. Munroe, *Supercond. Sci. Technol.* **15**, 1587 (2002).
- [4] A. Yamamoto, J. Shimoyama, S. Ueda, Y. Katsura, I. Iwayama, S. Horii, and K. Kishio, *Appl. Phys. Lett.* **86**, 212502 (2005).
- [5] M. Mudgel, V. Awana, H. Kishan, and G. Bhalla, *Solid State Commun.* **146**, 330 (2008).
- [6] V. Awana, A. Vajpayee, M. Mudgel, R. Rawat, S. Acharya, H. Kishan, E. Takayama-Muromachi, A. V. Narlikar, and I. Felner, *Phys. C (Amsterdam, Neth.)* **467**, 67 (2007).
- [7] E. Young and Y. Yang, *IEEE Trans. Appl. Supercond.* **17**, 2794 (2007).
- [8] T. Matsushita, *Flux Pinning in Superconductors*, Solid-State Sciences (Springer, Berlin, 2014), Vol. 146.
- [9] J. H. Kim, S. Oh, Y.-U. Heo, S. Hata, H. Kumakura, A. Matsumoto, M. Mitsuhashi, S. Choi, Y. Shimada, M. Maeda *et al.*, *NPG Asia Mater.* **4**, e3 (2012).
- [10] G. Papavassiliou, M. Pissas, M. Karayanni, M. Fardis, S. Koutandos, and K. Prassides, *Phys. Rev. B* **66**, 140514 (2002).
- [11] J. K. Jung, S. H. Baek, F. Borsa, S. L. Bud'ko, G. Lapertot, and P. C. Canfield, *Phys. Rev. B* **64**, 012514 (2001).
- [12] M. Saeed, K.-i. Kumagai, M. Filippi, and A. Bianconi, *J. Phys. Soc. Jpn.* **79**, 124711 (2010).
- [13] G. Papavassiliou, M. Pissas, M. Fardis, M. Karayanni, and C. Christides, *Phys. Rev. B* **65**, 012510 (2001).
- [14] M. Karayanni, G. Papavassiliou, M. Pissas, M. Fardis, K. Papagelis, K. Prassides, T. Takenobu, and Y. Iwasa, *J. Supercond.* **18**, 521 (2005).
- [15] S. Strässle, J. Roos, M. Mali, H. Keller, and J. Karpinski, *Phys. C (Amsterdam, Neth.)* **466**, 168 (2007).
- [16] K. Lee, K. Kang, B. Mean, M. Lee, J. Rhee, B. Cho, and J. Cho, *Phys. B (Amsterdam, Neth.)* **359–361**, 463 (2005).
- [17] T. Yamaji, M. Murakami, J. Fukazawa, T. Shimizu, and K. Takegoshi, *J. Phys. Soc. Jpn.* **77**, 044711 (2008).
- [18] P. Beckett, M. S. Denning, I. Heinmaa, M. C. Dimri, E. A. Young, R. Stern, and M. Carravetta, *J. Chem. Phys.* **137**, 114201 (2012).
- [19] M. Pissas, G. Papavassiliou, M. Karayanni, M. Fardis, I. Maurin, I. Margiolaki, K. Prassides, and C. Christides, *Phys. Rev. B* **65**, 184514 (2002).
- [20] K. Lee, B. Mean, K. Kang, and S. Kim, *J. Korean Phys. Soc.* **45**, 660 (2004).
- [21] K. Lee, K. Kang, B. Mean, M. Lee, and B. Cho, *J. Magn. Magn. Mater.* **272–276**, 165 (2004).
- [22] M. Mali, J. Roos, A. Shengelaya, H. Keller, and K. Conder, *Phys. Rev. B* **65**, 100518(R) (2002).
- [23] S. H. Baek, B. J. Suh, E. Pavarini, F. Borsa, R. G. Barnes, S. L. Bud'ko, and P. C. Canfield, *Phys. Rev. B* **66**, 104510 (2002).
- [24] S. L. Bud'ko, G. Lapertot, C. Petrovic, C. E. Cunningham, N. Anderson, and P. C. Canfield, *Phys. Rev. Lett.* **86**, 1877 (2001).
- [25] H. J. Choi, D. Roundy, H. Sun, M. L. Cohen, and S. G. Louie, *Nature (London)* **418**, 758 (2002).
- [26] L. Hebel and C. Slichter, *Phys. Rev.* **113**, 1504 (1959).
- [27] R. H. T. Wilke, S. L. Bud'ko, P. C. Canfield, D. K. Finnemore, R. J. Suplinskas, and S. T. Hannahs, *Phys. Rev. Lett.* **92**, 217003 (2004).
- [28] J.-P. Amoureux, C. Fernandez, and S. Steuernagel, *J. Magn. Reson., Ser. A* **123**, 116 (1996).
- [29] E. Hahn, *Phys. Rev.* **80**, 580 (1950).
- [30] C. R. Morcombe and K. W. Zilm, *J. Magn. Reson.* **162**, 479 (2003).
- [31] M. W. Pieper, H. Michor, M. Reissner, and T. Ali, *New J. Phys.* **15**, 053028 (2013).

- [32] B. Chen, P. Sengupta, W. P. Halperin, E. E. Sigmund, V. F. Mitrović, M. H. Lee, K. H. Kang, B. J. Mean, J. Y. Kim, and B. K. Cho, *New J. Phys.* **8**, 274 (2006).
- [33] J. M. Delrieu, *J. Phys. F* **3**, 893 (2001).
- [34] C. H. Recchia, C. H. Pennington, H. Hauglin, and G. P. Lafyatis, *Phys. Rev. B* **52**, 9746 (1995).
- [35] A. P. Reyes, X. P. Tang, H. N. Bachman, W. P. Halperin, J. A. Martindale, and P. C. Hammel, *Phys. Rev. B* **55**, R14737(R) (1997).
- [36] S. Serventi, G. Allodi, R. De Renzi, G. Guidi, L. Romanò, P. Manfrinetti, A. Palenzona, C. Niedermayer, A. Amato, and C. Baines, *Phys. Rev. Lett.* **93**, 217003 (2004).
- [37] C. Niedermayer, C. Bernhard, T. Holden, R. K. Kremer, and K. Ahn, *Phys. Rev. B* **65**, 094512 (2002).
- [38] E. H. Brandt, *Phys. Rev. B* **37**, 2349 (1988).
- [39] J. Korryng, *Physica* **16**, 601 (1950).
- [40] A. Gerashenko and K. Mikhalev, *Appl. Magn. Reson.* **21**, 157 (2001).
- [41] H. Kotegawa, K. Ishida, Y. Kitaoka, T. Muranaka, and J. Akimitsu, *Phys. Rev. Lett.* **87**, 127001 (2001).
- [42] K. Yosida, *Phys. Rev.* **110**, 769 (1958).
- [43] V. A. Stenger, C. H. Pennington, D. R. Buffinger, and R. P. Ziebarth, *Phys. Rev. Lett.* **74**, 1649 (1995).
- [44] S. Oh, A. M. Mounce, J. A. Lee, W. P. Halperin, C. L. Zhang, S. Carr, and P. Dai, *Phys. Rev. B* **87**, 174517 (2013).
- [45] T. Ekino, T. Takasaki, T. Muranaka, J. Akimitsu, and H. Fujii, *Phys. Rev. B* **67**, 094504 (2003).
- [46] T. Takasaki, T. Ekino, and T. Muranaka, *Phys. C (Amsterdam, Neth.)* **378–381**, 229 (2002).
- [47] P. Szabó, P. Samuely, J. Kačmarčík, T. Klein, J. Marcus, D. Fruchart, S. Miraglia, C. Marcenat, and A. G. M. Jansen, *Phys. Rev. Lett.* **87**, 137005 (2001).
- [48] H. Schmidt, K. E. Gray, D. G. Hinks, J. F. Zasadzinski, M. Avdeev, J. D. Jorgensen, and J. C. Burley, *Phys. Rev. B* **68**, 060508 (2003).
- [49] H. Kotegawa, K. Ishida, Y. Kitaoka, T. Muranaka, N. Nakagawa, H. Takagiwa, and J. Akimitsu, *Phys. Rev. B* **66**, 064516 (2002).
- [50] E. Pavarini and I. I. Mazin, *Phys. Rev. B* **64**, 140504(R) (2001).
- [51] S. Serventi, G. Allodi, C. Bucci, R. De Renzi, G. Guidi, E. Pavarini, P. Manfrinetti, and A. Palenzona, *Phys. Rev. B* **67**, 134518 (2003).
- [52] V. P. Antropov, I. I. Mazin, O. K. Andersen, A. I. Liechtenstein, and O. Jepsen, *Phys. Rev. B* **47**, 12373(R) (1993).